REPORT DOCUMENTATION PAGE

Form Approved OMB NO. 0704-0188

1. REPORT DATE (DD-MM-YYYY)	2. REPORT TYPE	3. DATES COVERED (From - To)
	New Reprint	-

4. TITLE AND SUBTITLE	5a. CONTRACT NUMBER
Special quasirandom structures to study the $(K_{0.5}Na_{0.5})NbO_3$ ...	W911NF-09-1-0435
	5b. GRANT NUMBER
	5c. PROGRAM ELEMENT NUMBER
	611103

6. AUTHORS

Brian K. Voas, Tedi-Marie Usher, Xiaoming Liu, Shen Li, Jacob L. Jones, Xiaoli Tan, Valentino R. Cooper, Scott P. Beckman

5d. PROJECT NUMBER

5e. TASK NUMBER

5f. WORK UNIT NUMBER

7. PERFORMING ORGANIZATION NAMES AND ADDRESSES	8. PERFORMING ORGANIZATION REPORT NUMBER
University of Florida Office of Engineering 339 Weil Hall Gainesville, FL 32611 -6550	

9. SPONSORING/MONITORING AGENCY NAME(S) AND ADDRESS (ES)	10. SPONSOR/MONITOR'S ACRONYM(S) ARO
U.S. Army Research Office P.O. Box 12211 Research Triangle Park, NC 27709-2211	11. SPONSOR/MONITOR'S REPORT NUMBER(S) 54169-MS-PCS.41

12. DISTRIBUTION AVAILIBILITY STATEMENT

Approved for public release; distribution is unlimited.

13. SUPPLEMENTARY NOTES

14. ABSTRACT

The local structure of $K_{0.5}Na_{0.5}NbO_3$ is investigated using first-principles methods with an optimized special quasirandom structure (SQS). Through a comparison of the computed pair distribution functions with those from neutron powder diffraction data, the SQS approach demonstrates its ability to accurately capture the local structure patterns derived from the random distribution of K and Na on the perovskite A-site. Using these structures, local variations in Na-O interactions are suggested to be the driving force behind the R3c to Pm phase transition. A comparison between the SQS and a rocksalt structure shows the inability of the latter to account for the local

15. SUBJECT TERMS

ferroelectric, computational modeling, lead-free piezoelectric, local structure

16. SECURITY CLASSIFICATION OF:			17. LIMITATION OF ABSTRACT	15. NUMBER OF PAGES	19a. NAME OF RESPONSIBLE PERSON
a. REPORT	b. ABSTRACT	c. THIS PAGE			Jacob Jones
UU	UU	UU	UU		19b. TELEPHONE NUMBER 919-515-4557

Report Title

Special quasirandom structures to study the $(\mathrm{K}_{0.5}\mathrm{Na}_{0.5})\mathrm{Nb}\mathrm{O}_3$ random alloy

ABSTRACT

The local structure of K0.5Na0.5NbO3 is investigated using first-principles methods with an optimized special quasirandom structure (SQS). Through a comparison of the computed pair distribution functions with those from neutron powder diffraction data, the SQS approach demonstrates its ability to accurately capture the local structure patterns derived from the random distribution of K and Na on the perovskite A-site. Using these structures, local variations in Na-O interactions are suggested to be the driving force behind the R3c to Pm phase transition. A comparison between the SQS and a rocksalt structure shows the inability of the latter to account for the local variability present in a random solid solution. As such, the predictive nature of the SQS demonstrated here suggests that this approach may provide insight in understanding the properties of a wide range of bulk oxide alloys or solid solutions.

REPORT DOCUMENTATION PAGE (SF298)
(Continuation Sheet)

Continuation for Block 13

ARO Report Number   54169.41-MS-PCS
Special quasirandom structures to study the <sp...

Special quasirandom structures to study the (K$_{0.5}$Na$_{0.5}$)NbO$_3$ random alloy

Brian K. Voas,[1] Tedi-Marie Usher,[2,3] Xiaoming Liu,[1] Shen Li,[1] Jacob L. Jones,[2,3] Xiaoli Tan,[1]
Valentino R. Cooper,[4,*] and Scott P. Beckman[1,†]

[1]*Department of Materials Science and Engineering, Iowa State University, Ames, Iowa 50011, USA*

[2]*Department of Materials Science and Engineering, University of Florida, Gainesville, Florida 36211, USA*

[3]*Department of Materials Science and Engineering, North Carolina State University, Raleigh, North Carolina 27695, USA*

[4]*Materials Science and Technology Division, Oak Ridge National Laboratory, Oak Ridge, Tennessee 37831, USA*

The local structure of K$_{0.5}$Na$_{0.5}$NbO$_3$ is investigated using first-principles methods with an optimized special quasirandom structure (SQS). Through a comparison of the computed pair distribution functions with those from neutron powder diffraction data, the SQS approach demonstrates its ability to accurately capture the local structure patterns derived from the random distribution of K and Na on the perovskite A-site. Using these structures, local variations in Na-O interactions are suggested to be the driving force behind the $R3c$ to Pm phase transition. A comparison between the SQS and a rocksalt structure shows the inability of the latter to account for the local variability present in a random solid solution. As such, the predictive nature of the SQS demonstrated here suggests that this approach may provide insight in understanding the properties of a wide range of bulk oxide alloys or solid solutions.

I. INTRODUCTION

A solid solution of KNbO$_3$ (KNO) with NaNbO$_3$ (NNO) was recently investigated as an environmentally friendly alternative to Pb containing Pb(Zr,Ti)O$_3$ (PZT) [1–3]. Similar to PZT, KNO-NNO shows a significant phase transition at a composition near (K$_{0.5}$Na$_{0.5}$)NbO$_3$ (KNN) [4]. While the change in phase is not mediated by a monoclinic phase and the piezoelectric response is still relatively low, understanding the nature of the electromechanical properties of this material near this phase boundary remains important for understanding this crystal family.

Given the relative chemical similarities between K and Na, it is anticipated that these cations will be distributed randomly on the perovskite A-site. Such random alloys represent a major challenge for first-principles calculations due to the limited size of the computational supercells that can be simulated. Typically, the structure and properties of an alloy are studied using small supercells, approximating the alloy compositions with highly ordered structures [5–7]. For compounds with simple ratios, like KNN, a rocksalt structure (RSS) is often used [8]. The RSS necessarily has short-ranged structural correlations that deviate significantly from those anticipated for a random structure, and these may have consequences for predicted macroscopic properties.

Although it is impossible to represent a truly random structure using a system with periodic boundary conditions, there exist several approaches to approximate the structure and behavior of random alloys. Mean-field methods, such as the virtual crystal approximation, do reproduce the properties in systems in which an averaging approach can be employed [9,10]. However, it is well known that variations in short-ranged chemical ordering, which are not expressed by these chemical averaging methods, play an important role in defining the behavior and properties of complex oxide ferroelectrics

[11–13]. Alternatively, interatomic potentials that can model large unit cells can account for the effects of local variations in bonding. These methods have been demonstrated to be successful at representing the physical properties of the ABO$_3$ perovskite compounds PZT [14] and BaTiO$_3$-SrTiO$_3$ [15,16]. Unfortunately, these approaches require extensive effort to parametrize the potentials and necessitate large experimental or computational datasets.

In this paper, first-principles density functional theory is used with the special quasirandom structure (SQS) [17] approach to explore the properties of the complex random alloy KNN. A SQS is designed by selectively populating a supercell such that the short-ranged, geometric correlations approximate that of the random alloy. Although this approach has been demonstrated to accurately reproduce the properties of metals [18–20] and semiconductors [21,22], it has only received minimal attention by the oxide community [23]. The predicted results from these computations are compared to structures measured from powered neutron diffraction experiments. This method gives pair distribution functions (PDFs) that are in excellent agreement with experimental low-temperature $R3c$ and room-temperature Pm phases. This is in stark contrast with the ground-state structures obtained using a typical RSS. Interestingly, the RSS produces a much broader distribution of cation-O and O-O displacement patterns. The SQS, however, shows that the polarization direction and hence the macroscopic phase/symmetry are correlated most strongly to local, nearest-neighbor, Na-O interactions that change most significantly between the ground-state $R3c$ and room-temperature Pm phases. This indicates that Na interactions are the driving force for the observed electromechanical responses in these materials.

II. METHODS

A. Theoretical methods

The structure and properties of the SQS and RSS supercells were calculated using density functional theory as

*coopervr@ornl.gov
†sbeckman@iastate.edu

TABLE I. The lattice vectors and atomic positions of the SQS in both absolute coordinates (scaled by a) and relative coordinates.

Lattice vectors		
$\vec{a}$	$\vec{b}$	$\vec{c}$
$(-1,1,1)$	$(1,-1,1)$	$(2,2,0)$
Atomic positions	Absolute	Relative
K atoms	(2,1,1)	(0.25,0.75,0.75)
	(1,2,1)	(0.75,0.25,0.75)
	(0,0,1)	(0.5,0.5,0)
	(1,1,1)	(0.5,0.5,0.5)
Na atoms	(1,0,1)	(0.25,0.75,0.25)
	(0,1,1)	(0.75,0.25,0.25)
	(0,0,0)	(0,0,0)
	(1,1,0)	(0,0,0.5)

implemented in the QUANTUM ESPRESSO software package [24]. Ultrasoft pseudopotentials were used in place of the all-electron ion potentials [25], and the exchange correlation energy was approximated using the local-density approximation (LDA) [26]. The Brillouin zone was sampled using a Monkhorst-Pack [27] $6 \times 6 \times 6$ k-point mesh, and the wave function was represented as a plane-wave expansion that was truncated at an energy of 100 Ry. Using these approximations, the atomic structures were optimized until the residual forces on the atoms were less than 5 meV/Å. The cubic lattice parameters for $KNbO_3$ and $NaNbO_3$ were calculated to be 3.95 and 3.91 Å, which agrees well with experiment [28,29]. Polarization and Born effective charges were calculated from density functional perturbation theory [30] and the Berry-phase technique [31].

The Alloy Theoretic Automated Toolkit (ATAT) [32] was used to produce SQSs with a 1 : 1 K:Na ratio. The SQSs generated had eight cubic unit cells with lattice parameter, a. The optimal SQS was selected as the one with the minimum root-mean-square deviation from the random pairwise correlations out to a distance of $6a$. It should be noted that although only one SQS was tested here, a total of five SQSs were found to have correlations that identically match the correlations for a random alloy out to third nearest neighbors, $a\sqrt{3}$. The selected SQS lattice vectors and unit cell occupations are listed in Table I and depicted in Fig. 1. The SQS is a superlattice in the [110] direction with a periodicity of $2\sqrt{2}a$. The stacking
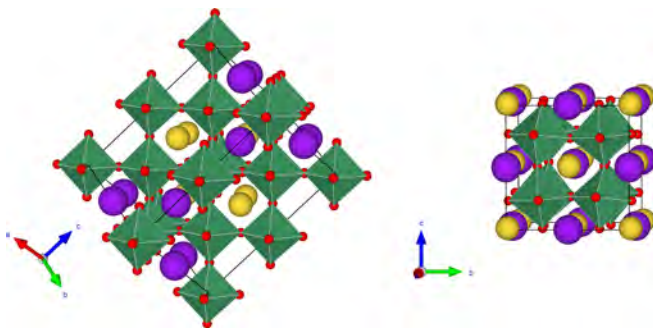

FIG. 1. (Color online) The atomic supercells used in these calculations to represent $\left(A'_{0.5}A''_{0.5}\right)BO_3$ perovskite random alloys. The SQS is shown on the left and the RSS on the right.

sequence is ... ,NaNa,NaK, KK, KNa,... , where NaNa refers to planes of all Na and NaK refers to planes containing alternating columns of Na and K sites aligned in the $[1\bar{1}\bar{1}]$ direction.

Both the $R3c$ and Pm phases were examined [33]. In both cases, the atomic structures were initialized according to their experimentally reported Glazer tilt patterns: $a_+^- a_+^- a_+^-$ for $R3c$ and $a_+^0 b_0^0 c_+^0$ for Pm [34]. The $R3c$ atomic structure was allowed to fully relax. The Pm phase was constrained to maintain its symmetry, which limited the atoms to moving only in the ac plane.

B. Experimental methods

For comparison, a set of KNN specimens was prepared by solid solution reaction methods and examined using neutron diffraction. The starting materials, Na_2CO_3 ($\geqslant$99.9%, Fisher), K_2CO_3 ($\geqslant$99.0%, Alfa Aesar), and Nb_2O_5 ($\geqslant$99.99%, Sigma-Aldrich), were stoichiometrically mixed in ethanol, and the resulting composition was then vibratory milled with zirconia milling media for 12 h. After drying for 20 h, the powders were calcined at 950 °C for 5 h. The composition and phase purity of the specimen were verified using a Siemens Model-D500 x-ray diffractometer. The resulting powder x-ray diffraction pattern for the KNN is shown in Fig. 2.

High-Q neutron powder diffraction data were collected on the NPDF instrument at the Los Alamos National Laboratory Lujan Neutron Scattering Center [35]. Approximately 10 g of KNN powder was loaded into a vanadium can, and measurements were performed at 15 and 300 K to allow for examination of both the rhombohedral and monoclinic phases. Using the program PDFGETN [36], standard data correction and normalization steps were performed, and the experimental pair distribution functions were extracted. Based on inspection of noise levels in the data, a wave-vector cutoff $Q_{\max}$ of 34 Å^{-1} was used.

III. RESULTS AND DISCUSSION

Reduced pair distribution functions (PDFs) from the experimental neutron powder diffraction data and from the
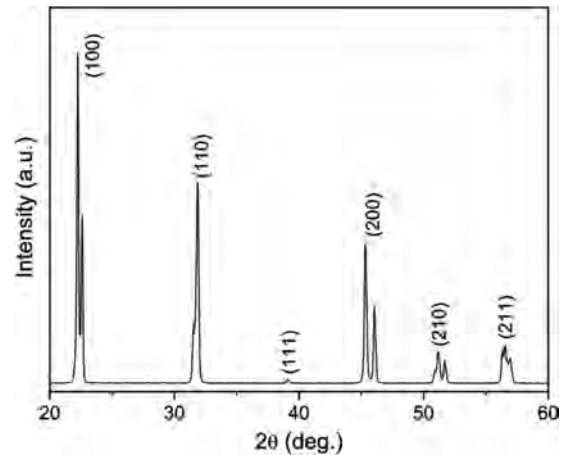

FIG. 2. The θ-2θ powder x-ray diffraction intensities taken for the calcined $(K_{0.5}Na_{0.5})NbO_3$ powder. The pattern indicates a single perovskite phase and is indexed based on the primitive cubic cell.
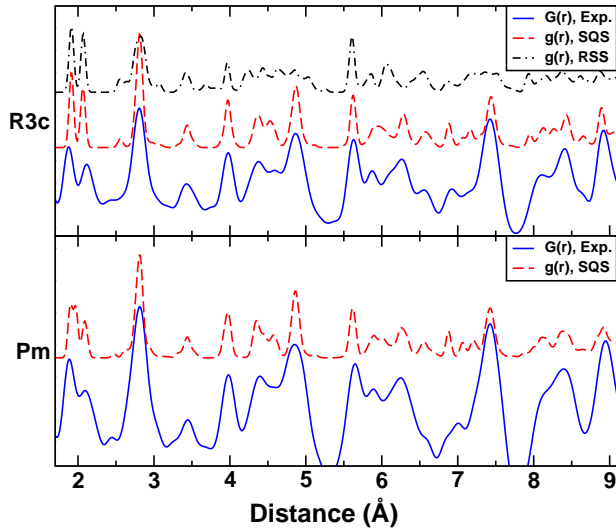
FIG. 3. (Color online) A comparison of the experimentally determined reduced PDF and the theoretical PDFs. The top frame shows the results for the rhombohedral phase and the bottom frame shows results from the monoclinic phase.

theoretical structures are compared in Fig. 3. The theoretical structures are linearly scaled by 1% to correct for the well-known LDA errors in lattice constants. The top frame of Fig. 3 shows results for the $R3c$ phase. The peak positions and relative intensities of the SQS are in excellent agreement with the experimental PDF obtained at 15 K. In contrast, the RSS PDF has spurious peaks and in several instances there are missing peaks. The results for the Pm phase, seen in the bottom frame of Fig. 3, further verify the ability of the SQS to predict the local structure of the KNN solid solution. The agreement between the SQS and experiment is again emphasized using the refined PDFs as shown in Fig. 4, in which the experimental data are modeled using the refined SQS structures and the PDFGUI software [37]. The refined PDFs clearly demonstrate the capacity of the SQS to provide a structural model for the KNN random alloy. Conversely, the RSS shows obvious
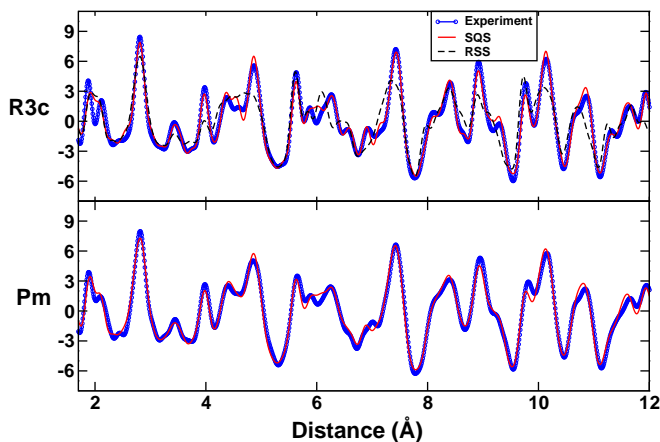

FIG. 4. (Color online) Refined PDFs for the $R3c$ (top) and Pm (bottom) phases.
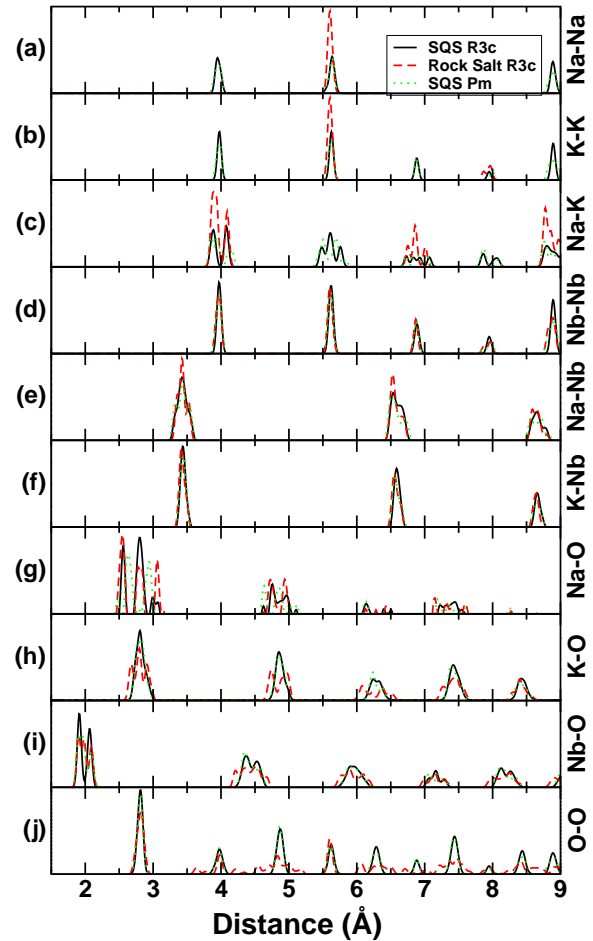

FIG. 5. (Color online) Partial pair-distribution functions for all atomic pairs. The solid black line is the SQS rhombohedral phase and the dashed red line is the RSS rhombohedral phase. The monoclinic phase for the SQS is shown as the dotted green line.

deficiencies that may be an indication of a poor representation of the random alloy.

An analysis of the SQS and RSS is performed by computing partial PDFs, shown in Fig. 5. This allows for an understanding of the pairwise relationships of these structures, as well as the underlying driving force behind the electromechanical responses. Figures 5(a)–5(c) shows the A-A-site cation interatomic distances. The large gaps between the peaks in the RSS data are due to the RSS ordering, that is, there exist no nearest-neighbor cations of the same composition, and all second-nearest neighbors have the same composition. The relative A-A-site cation interatomic distances are similar in all structures. In particular, K-K and Na-Na interactions all have narrow distributions indicating strong repulsion between these ions, in other words, collective motion, which undoubtedly sets the lattice constant of the KNN structure. Similar consideration of the nearest-neighbor Nb-Nb separations suggests a lattice parameter of 3.97 Å with a standard deviation of 0.015 Å. This is slightly larger than the predicted values for the bulk cubic, paraelectric, NNO, and KNO, and is a consequence of the polarization that develops in these unit cells. Nevertheless, in both the $R3c$ and the Pm structures there is a splitting of the nearest-neighbor Na-K peak. This is a result of larger

off-center displacements of Na cations than K. Interestingly, there is a shift in the relative peak separation between the two phases, as well as the presence of a third peak in the *Pm* phase. This is likely due to changes in the off-centering of the two sublattices, which induce physical changes in the direction of the macroscopic polarization of the material.

Similarly, sharp regularly spaced peaks are observed for *A-B* and Nb-Nb interactions, as shown in Figs. 5(d)–5(f), for both the *R3c* and *Pm* phases. Collectively, this is indicative of a global response of the cations, all displacing along the direction of the bulk polarization. Such a global response of cations to the overall polarization has been previously used to understand why the three composition-dependent phases of PZT have very similar PDFs but very different macroscopic polarizations [14]. In PZT, the overall macroscopic polarization was found to be due to a competition between local distortions due to ionic repulsion, primarily between Pb and Zr, and the cooperative displacement of the cations along the overall polarization direction [14]. Previous work of Suewattana and Singh indicates that in KNN, the *B-B*-site response is a result of stiff force constants between the *B*-site cations [38]. This is a direct result of *B*-O interactions where movement of *B*-site cations toward an O anion induces the neighboring *B*-cation to displace [39]. Unlike PZT, the competition between cations is minimized and only the collective motion of the ions defines the macroscopic polarization. This could be a reason for the low piezoelectric response observed in these materials, since it could be anticipated that the ionic responses to changes in the direction of the polarization would be far less than those found in PZT, where the changes in off-centering are much more dramatic.

Finally, the cation-oxygen and oxygen-oxygen bonding interactions are analyzed, as shown in Figs. 5(g) and 5(h). Interestingly, partial PDFs are similar for both the *R3c* and *Pm* phases for the interactions between K-O, Nb-O, and O-O. However, large deviations, especially for the nearest-neighbor distances, are observed in the Na-O PDFs between the *R3c* and *Pm* phases. Specifically, the three nearest-neighbor peaks in the *R3c* and the *Pm* phase are indicative of different displacement patterns. In the *R3c* phase, displacements are in the [111] direction, resulting in three short bonds (⩽2.65 Å), six medium length bonds (2.65–2.9 Å), and three long bonds (⩾2.9 Å) along this direction. On the other hand, in the *Pm* structure, the splitting in Na-O distances is manifested through the creation of one short bond along the [101] direction (⩽2.5 Å), four medium length bonds (2.5–2.75 Å), and seven long bonds (⩾2.75 Å). Despite these differences, the Na-O distances are governed by the preferred displacements of Na toward neighboring cells with K ions and away from those with Na cations. In other words, short Na-O bonds are observed in directions that are Na-O-K and longer bonds are in the direction of Na-O-Na bonds. This is also evident in the splitting of the Na-K peaks. Recent DFT studies comparing the cubic, paraelectric phases of KNO and NNO indicate significant changes in covalency and ionic charge transfer in KNO compared with NNO, with K resulting in more charge transfer to oxygen ions. This enhances the bond hybridization, which fosters off-centering and induces large cooperative displacements in nearby cations.

The observed changes in splitting are directly linked to the desire to displace in the direction of the overall polarization (or symmetry of the unit cell). This cooperative-competitive effect is very similar to that observed in PZT, and tuning this interaction may be useful in enhancing the ferroelectric nature of KNN.

It is important to point out that the results for the *R3c* obtained using the SQS method are in stark contrast with those of the RSS. A number of fundamental differences exist that change the interpretation of the origin of ferroelectric polarization in these materials. First, for the Na-O interactions there are only two bond distances. Although the displacements are still in the [111] directions, the lack of a third Na-O bond-distance splitting is indicative of a smaller magnitude of off-centering in this direction, shown in Fig. 5(g). Interestingly, there is now a more pronounced splitting in the K-O bond lengths, as demonstrated in Fig. 5(h), which suggests that the K cations now contribute more to the ferroelectricity in KNN, that is, larger off-centering, than indicated by the SQS. In addition, although there is no change in the computed Nb-O nearest-neighbor distances, there is a significant broadening of second-nearest-neighbor Nb-O bonds in the RSS versus the SQS, which is shown in Fig. 5(i). This is most likely linked to the large variation in the O-O bond distances, demonstrated in Fig. 5(j). This large variation is a strong indication of larger octahedral rotations. Such rotations are usually thought to counter the ferroelectric modes in these materials. Nevertheless, these observations suggest that by increasing the chemical complexity of the supercell, through a better approximation for the randomization of *A*-site cations, the variation in the bond-length distribution decreases.

Table II lists the Born effective charges, Z^*, and the magnitude of the polarization, P, for the *R3c* and *Pm* phases. The SQS method allows for accurate determination of the polarization. The contribution of each cation to the net dipole moment is characterized by determining the ions' displacement relative to the center of the nearest-neighbor oxygen cages, listed in Table II. On average, both SQS and RSS provide comparable results to the overall polarization. The variability of ionic displacement due to the local chemical environment is shown in Fig. 6. Cations in the SQS undergo larger relative displacements perpendicular to the bulk polarization direction, as would be expected in a random solution, yet these perpendicular components sufficiently cancel one another to allow the greatest contribution to be those components parallel to the macroscopic polarization. The RSS shows highly uniform deviation from

TABLE II. The Born effective charges, Z^*, in units of electron charge, angular deviation of cation displacement away from the bulk polarization direction, θ, in degrees, and polarization, P, in C/m^2.

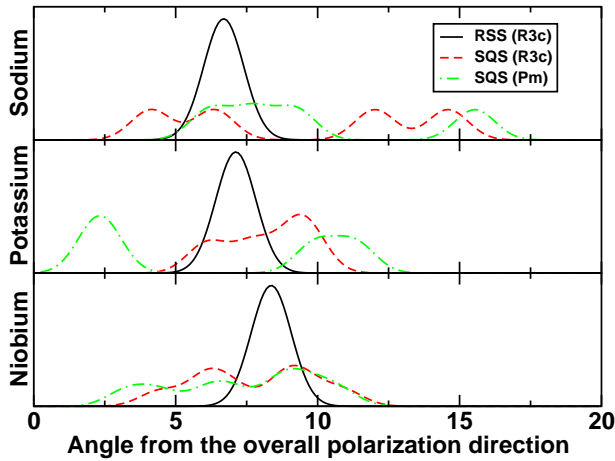|	Z^*			θ			
	K	Na	Nb	K	Na	Nb	P
RSS (*R3c*)	1.13	1.14	8.33	7.1	6.7	8.4	0.38
SQS (*R3c*)	1.15	1.15	8.38	8.2	9.3	7.8	0.39
SQS (*Pm*)	1.15	1.15	8.33	6.5	9.7	7.4	0.40

FIG. 6. (Color online) Distribution of cation distortion angles away from the bulk polarization direction of supercells for $R3c$ and Pm phases. The SQS supercells (broken lines) demonstrate greater variability in ionic contributions to overall polarization, while the RSS supercell (solid line) is highly uniform in its angular distribution.

individual cations due to the high symmetry imposed on the structure. The SQS is able to predict the bulk polarization while accounting for local influences due to the random environment.

The angular momentum and site-projected density of states for the relaxed structures are shown in Fig. 7. The valence band is primarily occupied by O p-states, and most of the Nb d-states exist in the conduction band. Hybridization between the Nb d-states and O p-states is evident from the presence of some Nb d-states within the valence band. The LDA band gaps for the ground-state SQS and RSS are 1.93 and 2.08 eV,
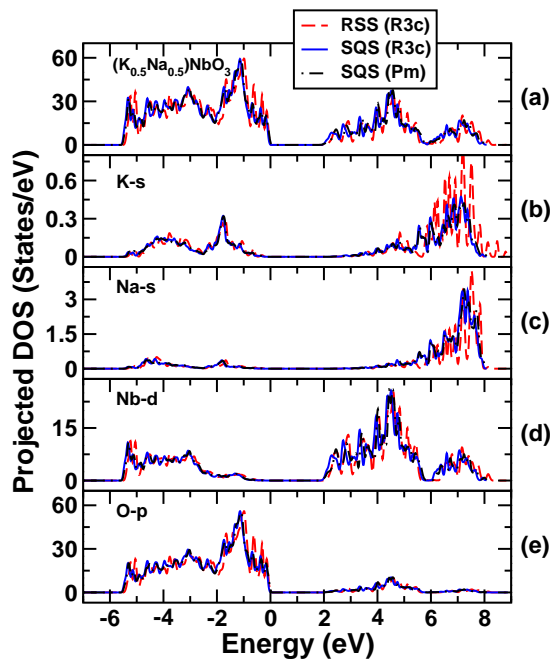

FIG. 7. (Color online) The projected density of states for the KNN relaxed structures. The origin has been placed at the top of the valence band.

respectively, while the Pm structure has a band gap of 1.87 eV, in comparison to an experimental band gap of 3.18 eV [40].

IV. SUMMARY AND CONCLUSIONS

In conclusion, the $R3c$ and Pm phases of the KNN random alloy are investigated using first-principles calculations. Using the SQS approach to construct supercells of KNN, one obtains PDFs that are in excellent agreement with those obtained from neutron diffraction experiments. This is in stark contrast with results for PDFs produced from supercells with the RSS. Using the SQS method, specific insights may be gained into the local structure interactions that control the physical properties of these materials. These results suggest that the ferroelectric polarization in these materials is governed by the cooperative-competitive interactions of Na. In particular, Na prefers to off-center in the direction of K cations and away from Na ions, while conforming as best as possible to the overall polarization direction. These interactions seem to be fundamental in perovskite oxide alloys and play an important role in defining the magnitude and direction of the macroscopic polarization. As such, these results highlight the effectiveness of a SQS for predicting the structures and properties of oxide solid solutions directly from first-principles calculations using relatively small supercells without resorting to the use of mean-field methods or parametrized interatomic potentials. This is paramount to the design of novel materials where macroscopic properties are strongly linked to the local atomic structure. The artificial, high-symmetry order of the RSS casts some doubts about using these wrongly correlated structures to predict the properties of perovskite compounds, although this approach is common. These results have clear consequences for first-principles discovery of novel materials with properties such as ferroelectricity, piezoelectricity, ferromagnetism, and thermoelectricity. For example, they suggest that the response of KNN may be enhanced through modifications that increase the bond frustration in these materials. One possibility may be through chemical pressure induced by the introduction of a larger cation such as Ta [41].

[1] C. W. Ahn, S. Y. Lee, H. J. Lee, A. Ullah, J. S. Bae, E. D. Jeong, J. S. Choi, B. H. Park, and I. W. Kim, J. Phys. D **42**, 215304 (2009).

[2] J. Tellier, B. Malic, B. Dkhil, D. Jenko, J. Cilensek, and M. Kosec, Solid State Sci. **11**, 320 (2009).

[3] L. Wu, J. L. Zhang, C. L. Wang, and J. C. Li, J. Appl. Phys. **103**, 084116 (2008).

[4] Y.-J. Dai, X.-W. Zhang, and K.-P. Chen, Appl. Phys. Lett. **94**, 042905 (2009).

[5] Z. Xin-Yin, W. Yue-Hua, Z. Min, Z. Na, G. Sai, and C. Qiong, Chin. Phys. Lett. **28**, 067101 (2011).

[6] V. R. Cooper, J. R. Morris, S. Takagi, and D. J. Singh, Chem. Mater. **24**, 4477 (2012).

[7] P. Marton and C. Elsaesser, Phys. Status Solidi B **248**, 2222 (2011).

[8] S. P. Beckman, X. Wang, K. M. Rabe, and D. Vanderbilt, Phys. Rev. B **79**, 144124 (2009).

[9] N. J. Ramer and A. M. Rappe, Phys. Rev. B **62**, R743 (2000).

[10] L. Bellaiche and D. Vanderbilt, Phys. Rev. B **61**, 7877 (2000).

[11] R. E. Cohen, Nature (London) **358**, 136 (1992).

[12] C. G. F. Stenger and A. J. Burggraaf, Phys. Status Solidi A **61**, 653 (1980).

[13] I. Grinberg, V. R. Cooper, and A. M. Rappe, Nature (London) **419**, 909 (2002).

[14] I. Grinberg, V. R. Cooper, and A. M. Rappe, Phys. Rev. B **69**, 144118 (2004).

[15] L. Walizer, S. Lisenkov, and L. Bellaiche, Phys. Rev. B **73**, 144105 (2006).

[16] M. Sepliarsky, A. Asthagiri, S. R. Phillpot, M. G. Stachiotti, and R. L. Migoni, Curr. Opin. Solid State Mater. Sci. **9**, 107 (2005).

[17] A. Zunger, S. H. Wei, L. G. Ferreira, and J. E. Bernard, Phys. Rev. Lett. **65**, 353 (1990).

[18] A. van de Walle, G. Ceder, and U. V. Waghmare, Phys. Rev. Lett. **80**, 4911 (1998).

[19] J. von Pezold, A. Dick, M. Friak, and J. Neugebauer, Phys. Rev. B **81**, 094203 (2010).

[20] V. Ozolins, C. Wolverton, and A. Zunger, Phys. Rev. B **57**, 6427 (1998).

[21] S. H. Wei and A. Zunger, Phys. Rev. Lett. **76**, 664 (1996).

[22] A. M. Saitta, S. de Gironcoli, and S. Baroni, Phys. Rev. Lett. **80**, 4939 (1998).

[23] A. I. Lebedev, Phys. Solid State **51**, 2324 (2009).

[24] P. Giannozzi, S. Baroni, N. Bonini, M. Calandra, R. Car, C. Cavazzoni, D. Ceresoli, G. L. Chiarotti, M. Cococcioni, I. Dabo, A. Dal Corso, S. de Gironcoli, S. Fabris, G. Fratesi, R. Gebauer, U. Gerstmann, C. Gougoussis, A. Kokalj, M. Lazzeri, L. Martin-Samos, N. Marzari, F. Mauri, R. Mazzarello, S. Paolini, A. Pasquarello, L. Paulatto, C. Sbraccia, S. Scandolo, G. Sclauzero, A. P. Seitsonen, A. Smogunov, P. Umari, and R. M. Wentzcovitch, J. Phys. Condens. Matter **21**, 395502 (2009).

[25] D. Vanderbilt, Phys. Rev. B **41**, 7892 (1990).

[26] J. P. Perdew and A. Zunger, Phys. Rev. B **23**, 5048 (1981).

[27] J. D. Pack and H. J. Monkhorst, Phys. Rev. B **16**, 1748 (1977).

[28] A. W. Hewat, J. Phys. C **6**, 2559 (1973).

[29] G. Shirane, H. Danner, A. Pavlovic, and R. Pepinsky, Phys. Rev. **93**, 672 (1954).

[30] X. Gonze and C. Lee, Phys. Rev. B **55**, 10355 (1997).

[31] F. Bernardini, V. Fiorentini, and D. Vanderbilt, Phys. Rev. B **56**, R10024 (1997).

[32] A. van de Walle, M. Asta, and G. Ceder, Calphad–Comput. Coupling Phase Diagrams Thermochem. **26**, 539 (2002).

[33] D. W. Baker, P. A. Thomas, N. Zhang, and A. M. Glazer, Appl. Phys. Lett. **95**, 091903 (2009).

[34] H. T. Stokes, E. H. Kisi, D. M. Hatch, and C. J. Howard, Acta Crystallogr. Sect. B **58**, 934 (2002).

[35] T. Proffen, T. Egami, S. J. L. Billinge, A. K. Cheetham, D. Louca, and J. B. Parise, Appl. Phys. A **74**, S163 (2002).

[36] P. F. Peterson, M. Gutmann, T. Proffen, and S. J. L. Billinge, J. Appl. Crystallogr. **33**, 1192 (2000).

[37] C. L. Farrow, P. Juhas, J. W. Liu, D. Bryndin, E. S. Bozin, J. Bloch, T. Proffen, and S. J. L. Billinge, J. Phys. Condens. Matter **19**, 335219 (2007).

[38] M. Suewattana and D. J. Singh, Phys. Rev. B **82**, 014114 (2010).

[39] I. Grinberg and A. M. Rappe, Phase Trans. **80**, 351 (2007).

[40] H. Jiang, T. T. Su, H. Gong, and Y. C. Zhai, Cryst. Res. Technol. **46**, 85 (2011).

[41] S. Y. Lee, C. W. Ahn, J. S. Kim, A. Ullah, H. J. Lee, H.-I. Hwang, J. S. Choi, B. H. Park, and I. W. Kim, J. Alloy. Compd. **509**, L194 (2011).